Poly(ethylene-2,6-naphthalate) Nanofiber Prepared by Carbon Dioxide Laser Supersonic Drawing

Akihiro Suzuki, Yuuki Yamada

Interdisciplinary Graduate of School of Medicine and Engineering, University of Yamanashi, Takeda-4, Kofu 400-8511 Japan

Received 16 April 2008; accepted 4 September 2008
DOI 10.1002/app.29805
Published online 7 January 2010 in Wiley InterScience (www.interscience.wiley.com).

ABSTRACT: Poly(ethylene-2,6-naphthalate) (PEN) nanofiber was prepared by a carbon dioxide (CO_2) laser supersonic drawing. The CO_2 laser supersonic drawing was carried out by irradiating the laser to the as-spun PEN fiber in a low-temperature supersonic jet. The supersonic jet was generated by blowing off air into a vacuum chamber from a fiber supplying orifice. The flow velocity from the orifice can be estimated by applying Graham's theorem from the pressure difference between the atmospheric pressure and the pressure of the vacuum chamber. The fastest flow velocity estimated was 396 m s^{-1} (Mach 1.15) at a chamber pressure of 6 KPa. The nanofiber obtained at Mach 1.15 was the oriented nanofibers with an average diameter of 0.259 μm, and its draw ratio estimated from the diameters before and after the drawing reached 430,822 times. The CO_2 laser supersonic drawing is a new method to make nanofiber without using any solvent or removing the second component.
 J Appl Polym Sci 116: 1913–1919, 2010

Key words: nanotechnology; polyesters; drawing

INTRODUCTION

Nanofibers are applied in a variety of fields such as membrane,[1–3] biomedical devices,[4] and scaffold for tissue engineering.[5–9] The nanofiber are prepared by an electrospinning,[10–13] sea-island-type conjugated melt spinning, single orifice melt blowing,[14] and a jet blowing.[15] The single orifice melt blowing and the jet blowing are new methods to prepare the nanofibers. The electrospinning is the method most often used for preparing the nanofibers at the moment. In the electrospinning, in the electric field between capillary tip and metallic collector, polymer solution is sprayed onto the metallic collector, and then made into nanofibers. In the sea-island-type conjugated melt spinning, the nanofiber is prepared by removing a sea component from the sea-island-type conjugated melt spun fiber.

A carbon dioxide (CO_2) laser-thinning method developed by us could easily produce microfibers by irradiating a continuous-wave CO_2 laser to fibers, such as poly(ethylene terephthalate) (PET),[16] nylon 6,[17] nylon 66,[18] i-polypropylene,[19] poly(L-lactic acid) (PLLA),[20,21] and poly(ethylene -2,6- naphthalate) (PEN)[22] fibers without highly skilled techniques. The microfiber obtained by winding on a spool in the winding speed range of 100–2500 m min^{-1} was monofilament microfiber with a uniform diameter. Furthermore, the CO_2 laser-thinning apparatus preparing the microfiber could be also produced the nonwoven fabric by using an air-jet and a collecting net in place of a winder. However, no fiber of 1 μm or less in the diameter of wound fiber and nonwoven fabric was obtained by the CO_2 laser-thinning method.

We developed a CO_2 laser supersonic drawing which is a new route to make nanofiber. In this approach, the nanofiber was obtained by CO_2 laser-irradiating an as-spun fiber in the low-temperature supersonic jet. The PET and PLLA nanofibers can be prepared by using the CO_2 laser supersonic drawing without using any solvent or removing the second component. Although the CO_2 laser supersonic drawing resembles the melt blowing in the point using a rapid air jet, the air jet generated by blowing off air into the vacuum chamber is the air flow without an accompanying flow. Unlike melt blown nanofiber, therefore, the nanofiber obtained by the laser-irradiation in the air flow without an accompanying flow is endless nanofiber with a uniform diameter. The supersonic drawing can be applied to almost all thermoplastic polymers in the same manner as the CO_2 laser-thinning method and is a novel method preparing the nanofibers.

We present here the results pertaining to the PEN nanofiber prepared by the CO_2 laser supersonic drawing.

Correspondence to: A. Suzuki (a-suzuki@yamanashi.ac.jp).
Contract grant sponsor: Scientific Research (B) of Japan Society for the Promotion of Science.

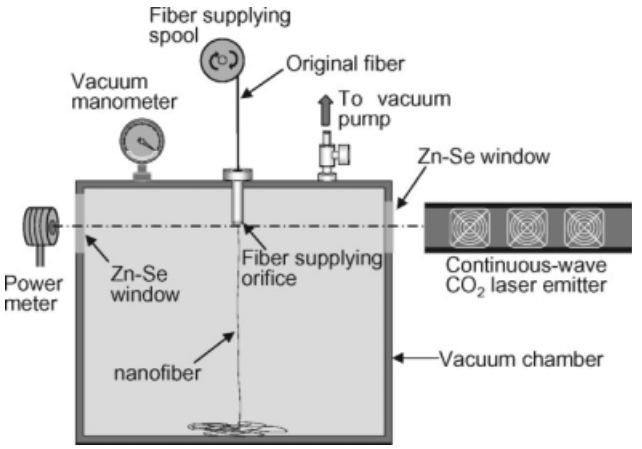

Figure 1 Schematic diagrams of apparatus used for the CO_2 laser supersonic drawing.

EXPERIMENTAL

The original PEN fiber used in the present study had a diameter of 170 μm, birefringence of 0.853 $\times$ 10^{-3}, and degree of crystallinity of 3% and was almost amorphous and isotropic fiber.

The morphology of nanofiber was determined with scanning electron microscopy (SEM). SEM micrographs of the fibers were observed with an accelerating voltage of 10 kV. Before the observation, the samples were coated with gold using a sputter coater. The average diameter and the diameter distribution were obtained by using imaging analyzer.

Wide-angle x-ray diffraction (WAXD) images of the nanofiber were taken with an imaging-plate (IP) film and an IP detector *R*-AXIS DS3C (Rigaku Co.). The IP film was attached to the X-ray generator (Rigaku Co.) operated at 40 kV and 200 mA. The radiation used was Ni-filtered CuK_α. The sample-to-film distance was 40 mm. The fiber was exposed for 5 min to the x-ray beam from a pinhole collimator with a diameter of 0.4 mm.

The DSC measurements were carried out using a THERM PLUS 2 DSC 8230C calorimeter (Rigaku Co.). The DSC scans were performed within the temperature range of 25 to 300°C using a heating rate of 10°C min^{-1}. All DSC experiments were carried out under a nitrogen purge. About 2 mg of nanofiber mat was sealed in aluminum pan and used for the measurement. The DSC instrument was calibrated with indium. The degree of crystallinity (X_c) was determined from heat of fusion (ΔH_m) and enthalpy of cold crystallization (ΔH_{cc}) as follows

$$X_c(\%) = [(\Delta H_m + \Delta H_{cc})/ - 190] \times 100$$

where -190 J g^{-1} is used as the heat of fusion of the crystalline phase of PEN.[23]

The apparatus used for the CO_2 laser supersonic drawing consisted of spool supplying the original fiber, a continuous wave CO_2 laser emitter (a wave number of 10.6 μm, a beam diameter of 2.4 mm), the vacuum chamber with antireflection coating Zn-Se windows, fiber supplying orifice with a diameter of 0.5 mm, power meter, and a vacuum pump as shown in Figure 1. The laser power of more than 90% was obtained in the area of the 2.4-mm ϕ laser spot. The power intensity was estimated by dividing the measured laser power in the area of the laser spot. The maximum laser intensity in this study was 177 W cm^{-2}. The original fiber was laser-irradiated at a point about 3 mm away from the orifice.

FLOW VELOCITY IN SUPERSONIC JET

Figure 2 shows the schematic diagram for free expansion of air in the supersonic jet. The air flow from the orifice occurred by the pressure difference across the orifice when the vacuum chamber was exhausted by the vacuum pomp. The flow velocity (v) from the orifice can be estimated by applying Graham's theorem:

$$v = \left\{\frac{2(p_0 - p)}{\rho}\right\}^{\frac{1}{2}} \quad (1)$$

where p_0 is atmospheric pressure, p is the pressure of the vacuum chamber, and the ρ is air density (= 1.2 g L^{-1}). The flow velocity is converted into a Mach number by dividing it by the sonic speed at a temperature of T_0:

$$M = \frac{v}{C} = \frac{v}{331.5 + 0.6(T_0 - 273.5)} \quad (2)$$

The adiabatic expansion of air across the orifice causes the decrease in the temperature of jet. Because the conservation law of energy along the streamlines exists in this case, the following

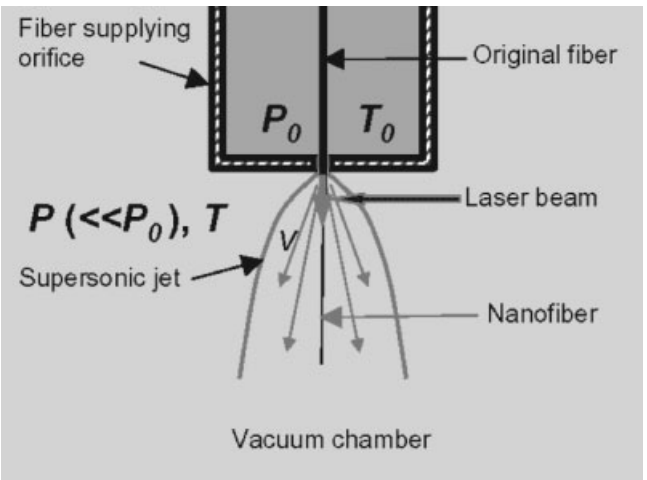

Figure 2 Free air expansion into vacuum chamber.

TABLE I
Flow Velocity (v), Mach Number (M) at 298.5 K, Temperature of Supersonic Jet (T) Estimated at Four Different Chamber Pressures (p)

p (KPa)	v (m s^{-1})	M at 298.5 K	T (K)
40	316	0.92	258
30	342	0.99	250
20	365	1.05	244
6	396	1.15	236

functional relation holds true between the ratio of temperatures before (T_0) and after (T) the adiabatic expansion and the Mach number (M)[24]:

$$\frac{T}{T_0} = \left\{1 + \frac{(\gamma - 1)M^2}{2}\right\}^{-1} \quad (3)$$

where γ ($= C_p/C_v$) is the ratio of heat capacity at constant pressure (C_p) and that at constant volume (C_v), and the γ value is 1.4 because air is a diatomic gas.

Table I lists the flow velocity (v) estimated by eq. (1), the Mach number at 298.5 K by eq. (2), and the temperature (T) of supersonic jet by eq. (3) at four different chamber pressures (p). As the chamber pressure decreases, the flow velocity increased and reaches 396 m s^{-1} (Mach 1.15) at a chamber pressure of 6 KPa, and the temperature of supersonic jet drops into 236.1 K.

RESULTS AND DISCUSSION

The fiber diameter in the CO_2 laser supersonic drawing depends on the chamber pressure, the laser intensity, and the supplying speed. To confirm the effect of their experimental conditions on the fiber diameter and its superstructure, the fibers drawn by changing their experimental factors were characterized by SEM, WAXD, and DSC measurements.

Figure 3 shows the chamber pressure dependence of the average diameters of fibers obtained at three different laser intensities. A series of experiments were carried out at a fiber supplying speed of 0.1 m min^{-1}. The fiber diameter at each the laser intensity decreases as the chamber pressure decreases, and the only fibers drawn under a chamber pressure of 6 KPa have an average diameter of less than 1 μm at all the laser intensities. The fiber was not drawn by the laser-irradiating at a laser intensity of 89 W cm^{-2} under a chamber pressure of 40 KPa.

Table II lists the average diameter, minimum and maximum diameters, and standard deviation for the fibers drawn by changing the chamber pressure. The supplying speed and the laser intensity were kept constant at 0.1 m min^{-1} and 177 W cm^{-2}, respectively. The decrease in the chamber pressure led to a decrease in the average diameter, minimum and maximum diameters, and standard deviation. The

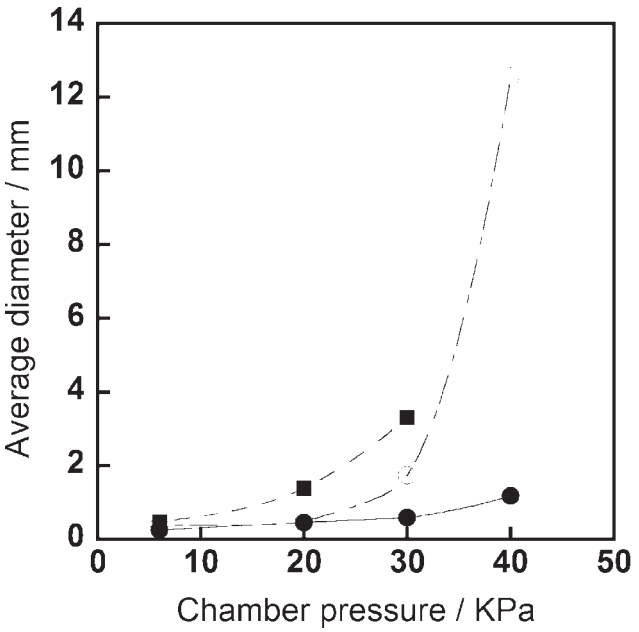

Figure 3 Chamber pressure dependence of average diameter of the fibers obtained at various laser intensities (I), ■: I = 89 W cm^{-2}, ○: I = 133 W cm^{-2}, ●: I = 177 W cm^{-2}.

nanofiber with an average diameter of 0.259 μm was obtained when the chamber pressure was 6 KPa, its minimum and maximum diameters are 0.120 μm and 0.400 μm, and the standard deviation is 0.054.

Figure 4 shows the diameter distributions of the fibers obtained by irradiating the laser at 177 W cm^{-2} to the original fiber supplied at 0.1 m min^{-1} at four different chamber pressures. The diameter distributions become gradually narrow, and the fiber diameter decreases as the chamber pressure decreases. The thinner the fiber diameter, the higher the uniformity of nanofiber becomes.

The decrease in the camber pressure increases the flow velocity from the orifice. The increase in the flow velocity increases the drag force and decreases the temperature in the air jet. The drag force has effects upon not only the fiber diameter but also the degree of molecular orientation and degree of crystallinity. The air flow behavior turns to a turbulent flow as the chamber pressure increases because of an accompanying flow. The uniformity of the

TABLE II
Average Diameter (d_{av}), Maximum Diameter (d_{max}), Minimum Diameter (d_{min}), and Standard Deviation (σ) for the Fibers Obtained at Four Different Chamber Pressures (p)

p (KPa)	d_{av} (μm)	d_{max} (μm)	d_{min} (μm)	σ
40	1.186	1.720	0.850	0.187
30	0.595	0.760	0.420	0.064
20	0.463	0.660	0.330	0.062
6	0.259	0.400	0.120	0.054

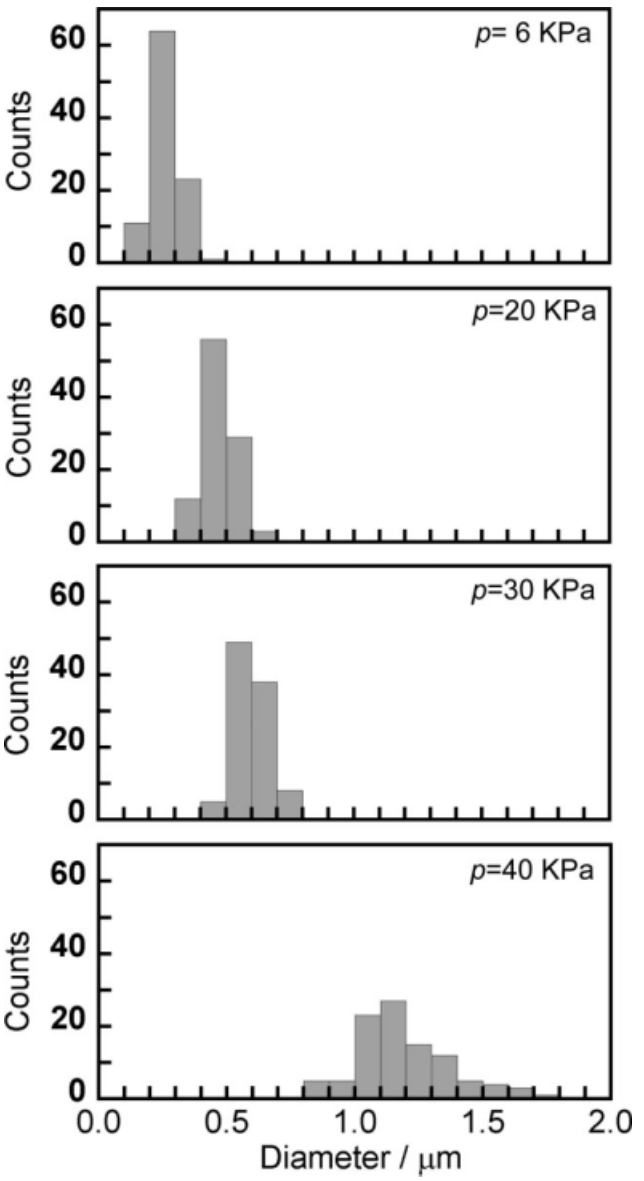

Figure 4 Diameter distributions of the fibers obtained at four different chamber pressures (p), laser intensity of 177 W cm^{-2}, and supplying speed of 0.1 m min^{-1}.

nanofiber decreases because the fiber at the laser-irradiating point is swayed by the turbulent flow. The lower chamber pressure is necessary to make the nanofiber with the uniform diameter.

Figure 5 shows the SEM micrographs of 3,000 magnifications for the fibers obtained by varying the chamber pressure. As the chamber pressure increases, the decrease in the diameter and the increase in the uniformity of fiber are confirmed visually by their SEM micrographs. The observation by the SEM micrographs shows that the nanofiber has a smooth surface without a surface roughened by a laser-ablation, and there is no droplet.

It is well known that the molecular weight decreases by the thermal degradation occurred during the melt spinning. In the previous study,[18] to examine whether the thermal degradation during the CO_2 laser-irradiating occurred or not, the GPC measurements were carried out for the nylon 66 microfiber obtained by the CO_2 laser-thinning. The results implied that molecular weight of the nylon 66 did not change before and after the laser irradiation. The only point locally molten by irradiating the high output power laser was deformed largely momentarily, and the nylon 66 microfiber was formed without the thermal degradation. It is thought that the thermal degradation hardly occurred during the laser supersonic drawing because the laser-irradiation to the fiber was performed by short time (< about 1 s) in the same manner as the laser-thinning method.

Henceforth the CO_2 laser supersonic drawing was carried out only at 6 KPa because the lowest chamber pressure was more effective in attenuating the PEN fiber. To confirm the effect of the supplying speed and the laser intensity on attenuating the fiber at constant chamber pressure, the CO_2 laser supersonic drawing was carried out by varying their experimental conditions.

Figure 6 shows the supplying speed dependence of the average diameter of the fibers obtained at various laser intensities. As supplying speed decreases, the fiber diameter at each laser intensity is tending to decrease, and the nanofiber with an average diameter of 0.259 μm is obtained when the original fiber supplied at a speed of 0.1 m min^{-1} was laser-irradiated at a laser intensity of 177 W cm^{-2}.

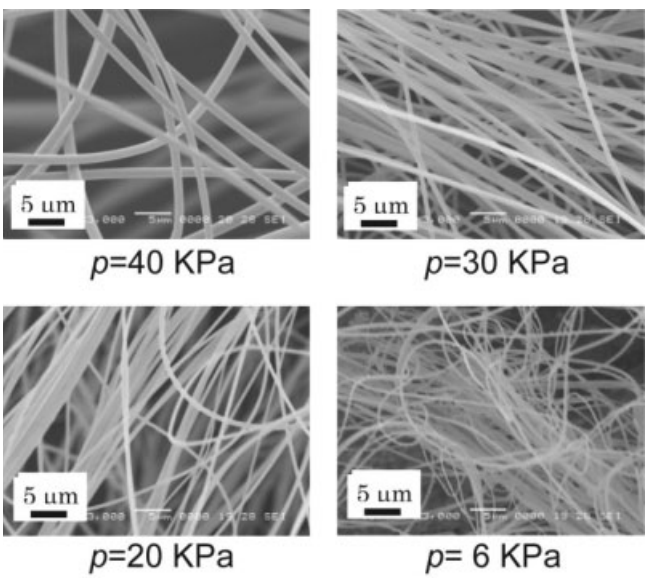

Figure 5 SEM photograph of 3,000 magnifications for the fibers obtained at four different chamber pressures, laser intensity of 177 W cm^{-2}, and supplying speed of 0.1 m min^{-1}.

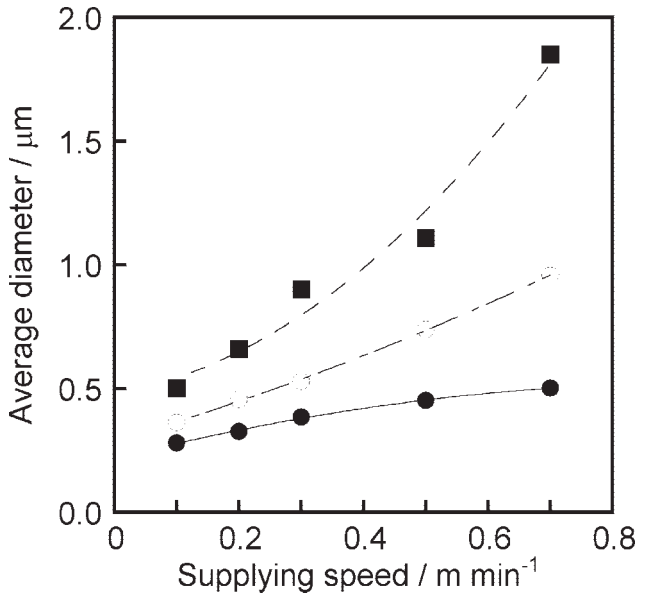

Figure 6 Supplying speed dependence of average diameter of the fibers obtained at various laser intensities (I), ■: I = 89 W cm^{-2}, ○: I = 133 W cm^{-2}, ●: *I = 177 W cm^{-2}.

The draw ratio (λ) can be calculated easily using the following equation

$$\lambda = \left(\frac{d_0}{d}\right)^2 \tag{4}$$

where d_0 is the diameter of the original fiber and d is that of the nanofiber, and the volumes before and after the drawing are assumed to be constant. The estimated draw ratio of the thinnest nanofiber reaches 430,822 times. A very large plastic deformation occurred momentarily in the low-temperature supersonic jet.

The irradiation of the higher output laser lowers the polymer viscosity instantly, and the polymer flow rate increases. The decrease in the supplying speed reduces the polymer mass supply to the laser irradiation position. The deformation of the molten polymer becomes larger because the same drag force acts on the less polymer mass molten by the laser irradiation. Furthermore, the relaxation of molecular chain oriented along the fiber axis by a flow-induced orientation does not occur because of the instantaneous laser irradiation in the low-temperature supersonic jet.

Figure 7 shows WAXD patterns of PEN nanofiber obtained at various supplying speeds. The laser intensity and the chamber pressure during one series of experiments were kept 177 W cm^{-2} and 6 KPa, respectively. No reflection due to the crystallites is observed in their WAXD patterns. Debye-Scherrer rings would appear in the WAXD because the nanofiber mat was used for their measurements if the crystallites existed in the supersonic drawn PEN nanofibers. The existence of the crystallites in the supersonic drawn fibers was not confirmed from their WAXD images, but the result of the DSC measurements described below suggests that the crystallites formed by the flow-induced crystallization slightly exist in the nanofibers.

Figure 8 shows DSC curves for the original fiber and the fibers obtained by four different supplying speeds, and their enthalpy of cold crystallization (ΔH_{cc}), heat of fusion (ΔH_m), and degree of crystallinity (X_c) estimated from ΔH_{cc} and ΔH_m values are shown in Table III. The laser intensity and the chamber pressure were kept constant at 177 W cm^{-2} and 6 KPa, respectively.

The original fiber had a cold crystallization temperature (T_{cc}) of 212°C, a melting point (T_m) of 266°C, and a degree of crystallinity of 3%. The T_{cc} of PEN is higher than that (about 130°C) of PET although the chemical structure of PEN and PET is closely resemble. The melting peak can be ascribed to the lamellar crystals which crystallized during the DSC scanning.[25,26]

The T_{cc} decreased with decreasing the supplying speed, and that of the nanofiber obtained at $S_s = 0.5$ m min^{-1} was 164°C, and the T_{cc}s of other nanofibers

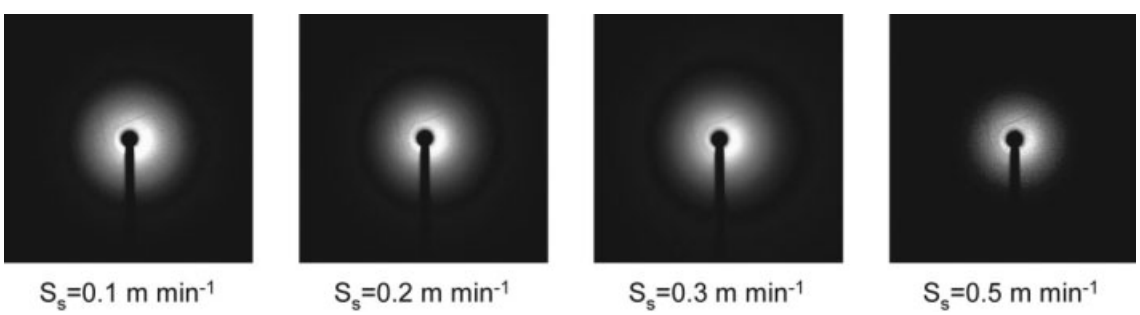

Figure 7 Wide angle X-ray diffraction patterns of PEN nanofiber obtained at various supplying speeds (Ss), laser power density of 177 W cm^{-2}, and chamber pressure of 6 KPa.

were observed in the temperature range, 156°C–159°C. The shifting of T_{cc} to the lower temperature is caused by the increase in the degree of orientation of amorphous chains and the existence of the crystal seeds. The drop in the T_{cc} of the supersonic drawn nanofiber indicates that the amorphous chains were oriented along the fiber axis by the flow-induced orientation and that the crystal seeds were formed during the supersonic drawing.

The T_ms of all nanofibers are lower than that (266°C) of the original fiber. The crystal from were roughly classified into a fringed-micelle crystal and the lamellar crystal. The former is formed by the strain-induced crystallization, the latter is induced by the annealing under a tensionless and during the DSC scanning. The T_m of the fringed-micelle crystal is lower than that of the lamella. Elenga et al.[27] suggested from the standpoint of kinetics that the low-temperature melting peak was ascribed to the fringed-micelle crystals built up by chain unfolding, and the high-temperature one corresponds to the untransformed fraction of the that undergo reorganization during the heating scan.

The melting peaks observed in the PEN nanofibers were attributed to the fringed-micelle crystal because their melting peaks were lower than that of the original fiber. The DSC behavior suggests that the oriented fringed-micelle crystalline seeds, which were formed by the rapid flow, grow in the fiber axis during the DSC scanning.

TABLE III
Enthalpy of Cold Crystallization (ΔH_{cc}), Heat of Fusion (ΔH_m), and Degree of Crystallinity (X_c) Estimated from ΔH_{cc} and ΔH_m Values for the Original Fiber and the Nanofibers Obtained at Four Different Supplying Speeds (S_s)

Fiber	ΔH_{cc} (J g^{-1})	ΔH_m (J g^{-1})	X_c (%)
Original	40.27	−45.26	3
S_s = 0.1 m min^{-1}	23.42	−52.87	16
=0.2 m min^{-1}	26.40	−56.50	16
=0.3 m min^{-1}	29.72	−60.13	16
=0.5 m min^{-1}	26.06	−59.37	18

All nanofiber obtained have a degree of crystallinity ranging from 16 to 18%, and their DSC data show that the flow-induced crystallization takes place during the supersonic drawing unlike the WAXD measurement. The morphological fine particles such as the crystalline seed and small crystallites can hardly be detected by the WAXD measurement. It has been found by many previous experiments that the detectable reflection due to the crystallites appears when the degree of crystallinity reaches higher than 30%.

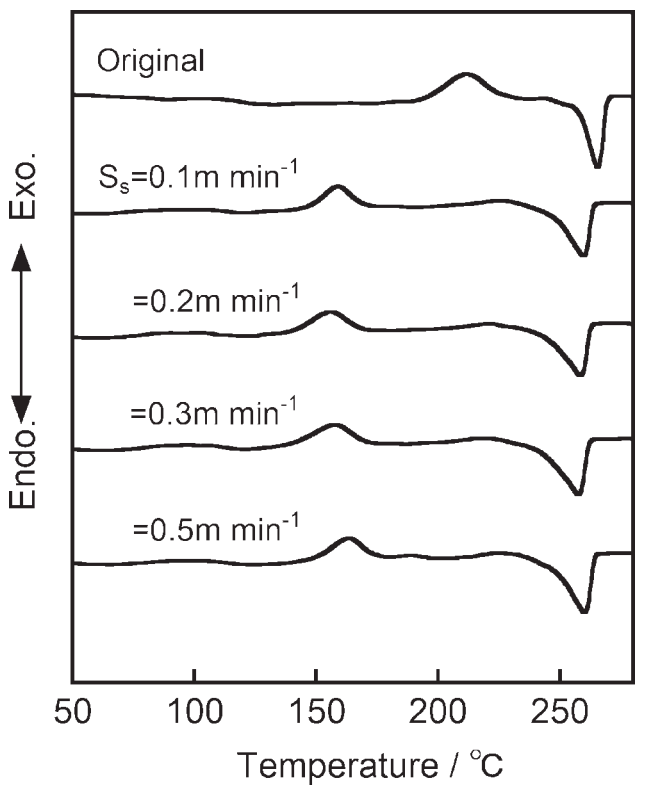

Figure 8 DSC curves for the original fiber and the fibers obtained at four different supplying speeds at a laser intensity of 177 W cm^{-2} and chamber pressure of 6 KPa.

CONCLUSIONS

We have shown that the monofilament PEN nanofiber with the uniform diameter was continuously obtained by the CO_2 laser supersonic drawing in the low-temperature supersonic jet. The CO_2 laser supersonic drawing could easily produce monofilament PEN nanofibers without using any solvent or removing the second component and can also be widely applied to thermoplastic polymers. The CO_2 laser supersonic drawing is a novel method preparing the nanofibers.

References

1. Yeo, Y.; Jeon, D.; Kim, C.; Choi, S.; Cho, K.; Lee, Y.; Kim, C. J Biomed Mater Res B 2005, 72, 86.
2. Lee, K.; Givens, S.; Chase, D. B.; Rabolt, J. F. Polymer, 2006, 47, 8013.
3. Zong, X.; Kim, K.; Fang, D.; Ran, S.; Hsiao, B. S.; Chu, B. Polymer, 2002, 43, 4403.
4. Meng, J.; Song, L.; Meng, J.; Kong, H.; Zhu, G.; Wang, C.; Xu, L.; Xie, S.; Xu, H. J Biomed Mater Res A 2006, 79, 298.
5. You, Y.; Min, B. M.; Lee, S. J.; Lee, T. S.; Park, W. H. J Appl Polym Sci 2005, 95, 193.
6. Kim, B.S.; Mooney, D. J. J Biomed Mater Res 1998, 41, 322.
7. Higgins, S. P.; Solan, A. K.; Niklason, L. E. J Biomed Mater A 2003, 67, 295.
8. Jinming, G.; Niklason, L.; Langer, R. J Biomed Mater Res 1998, 42, 417.
9. Eugene, D. B.; Todd, A. T.; David, G. S.; Gary, E. W.; Gary, L. B. J Biomed Mater Res B 2004, 71, 144.

10. Ding, B.; Kimura, E.; Satoa, T.; Fujita, S.; Shiratori, S. Polymer 2004, 45, 1895.
11. Gupta, P.; Wilkes, G. L. Polymer 2003, 44, 6353.
12. Ayutsede, J.; Gandhi, M.; Sukigara, S.; Micklus, M.; Chen, H. E.; Ko, F. Polymer 2005, 46, 1625.
13. Fong, H. Polymer 2004, 45, 2427.
14. Ellison, C. J.; Phatak, A.; Giles, D. W.; Macosko, C. W.; Bates, F. S. Polymer 2007, 48, 3306.
15. Borkar, S.; Gu, B.; Dirmyer, M.; Delicado, R.; Sen, A. N.; Jackson, B. R.; Badding, J. V. Polymer 2006, 47, 8337.
16. Suzuki, A.; Okano, T. J Appl Polym Sci 2004 92, 2989.
17. Suzuki, A.; Kamata, K. J Appl Polym Sci 2004, 92, 1454.
18. Suzuki, A.; Hasegawa, T. J Appl Polym Sci 2006, 101, 42.
19. Suzuki, A.; Narisue, S. J Appl Polym Sci 2006, 99, 27.
20. Suzuki, A.; Mizuochi, D.; Hasegawa, T. Polymer 2005, 46, 5550.
21. Suzuki, A.; Mizuochi, D. J Appl Polym Sci 2006, 102, 472.
22. Suzuki, A.; Tojyo, M. Eur Polym J 2007, 43, 2922.
23. Büchner, S.; Wiswe, D.; Zachmann, H. G. Polymer 1989, 30, 480.
24. Hagena, O. F. Surf Sci 1981, 106, 101.
25. Quintanilla, L.; Rodriguez-Cabello, J. C.; Pastor, J. M. Polymer 1994, 35, 2321.
26. Sawai, D.; Takahashi, K.; Imamura, T.; Nakamura, K.; Kanamoto, T.; Hyon, S. H. J. Polym Sci Part B: Polym Phys 2002, 40, 95.
27. Elenga, R.; Seguela, R.; Rietsch, F. Polymer 1991, 32, 1975.